Nuclear Inst. and Methods in Physics Research, A 893 (2018) 157–163

Contents lists available at ScienceDirect

Nuclear Inst. and Methods in Physics Research, A

journal homepage: www.elsevier.com/locate/nima

Thermal neutron detector based on COTS CMOS imagers and a conversion layer containing Gadolinium

Martín Pérez [a,b,*], Juan Jerónimo Blostein [b,c], Fabricio Alcalde Bessia [b,c], Aureliano Tartaglione [c,d], Iván Sidelnik [b,c], Miguel Sofo Haro [b,c], Sergio Suárez [a,b,c], Melisa Lucía Gimenez [a,b], Mariano Gómez Berisso [b,c], Jose Lipovetzky [a,b,c]

[a] Comisión Nacional de Energía Atómica, Argentina
[b] Instituto Balseiro, Universidad Nacional de Cuyo, Argentina
[c] Consejo Nacional de Investigaciones Científicas y Técnicas, Argentina
[d] Instituto Dan Beninson, Universidad Nacional de San Martín, Argentina

ARTICLE INFO

MSC:
00-01
99-00

Keywords:
CMOS sensors
Position sensitive neutron detectors
Gadolinium conversion layer
Neutron detection technique

ABSTRACT

In this work we will introduce a novel low cost position sensitive thermal neutron detection technique, based on a Commercial Off The Shelf CMOS image sensor covered with a Gadolinium containing conversion layer. The feasibility of the neutron detection technique implemented in this work has been experimentally demonstrated. A thermal neutron detection efficiency of 11.3% has been experimentally obtained with a conversion layer of 11.6 μm. It was experimentally verified that the thermal neutron detection efficiency of this technique is independent on the intensity of the incident thermal neutron flux, which was confirmed for conversion layers of different thicknesses. Based on the experimental results, a spatial resolution better than 25 μm is expected. This spatial resolution makes the proposed technique specially useful for neutron beam characterization, neutron beam dosimetry, high resolution neutron imaging, and several neutron scattering techniques.

1. Introduction

Thermal neutron detection has important applications in nuclear instrumentation, neutron techniques, particle physics, radiation safety, etc. In addition, during the last decade neutron detection has become also important for homeland security. Neutron detectors based on ^{3}He, which had been widely used for research during the last decades, where then installed at the US borders in order to prevent the illegal traffic of radioactive materials [1]. The current demand for ^{3}He for neutron detectors and other systems has created a shortage of this gas. Therefore, an alternative technology for neutron detection without using ^{3}He is required nowadays [1–4]. Besides, it is worth to mention that several neutron techniques employed for the study of condensed matter could be significantly improved if high spatial resolution detectors were available [5,6].

In this context, during the last years different detection techniques were developed for neutron detection using semiconductors [3,7–12]. This kind of detectors provide a compact technology for different neutron detection techniques. Such devices can be produced by coating a semiconductor – which is sensitive to charged particles – with a film that converts neutrons into charged particles. Commonly used films for such devices utilize the ^{10}B(n,α)^{7}Li reaction or the ^{6}Li(n,α)^{3}H reaction [8].

Ref. [13] shows an array of silicon detectors built with pyramidal dips, covered with ^{6}LiF. Refs. [9,14] shows etched pillars of P–I–N diodes immersed in a ^{10}B layer. These geometries allow to increase the conversion layer thickness – and therefore the neutron capture probability– , as well as the collection capability of the charged particles emitted after the nuclear reaction.

In a previous work [3], we propose the thermal neutron detection by using a scientific Charge Coupled Device (CCD) covered with a boron enriched layer. When a thermal neutron interacts with the conversion layer, charged particles are generated after the nuclear reaction ^{10}B(n,α)^{7}Li. These particles, with energies in the range of 0.5 – 5.5 MeV, produce a plasma effect in the CCD which is recorded as a circular spot in the image. That work shows that a spatial resolution of approximately 15 micrometer can be reached with the mentioned technique. However, these detectors have a high cost, and must be refrigerated with liquid Nitrogen to reduce the dark noise. Last mentioned characteristics strongly reduce its field of application.

* Correspondence to: Centro Atómico Bariloche, Av. Bustillo 9500, S. C. de Bariloche, 8400, Rio Negro, Argentina.
E-mail address: martin.perez@ib.edu.ar (M. Pérez).

https://doi.org/10.1016/j.nima.2018.03.032
Received 17 January 2018; Received in revised form 26 February 2018; Accepted 10 March 2018
Available online 20 March 2018
0168-9002/© 2018 Elsevier B.V. All rights reserved.

In previous works [15,16] we have analyzed the response of two different Commercial Off The Shelf (COTS) Complementary Metal Oxide Semiconductor (CMOS) image sensors as particle detector. When a charged particle interacts with the sensor active volume, it ionizes atoms producing a cluster of pixels with a intensity higher than a background level. The CMOS image sensors based on Active Pixel Sensors (APS) arrays are widely used in commercial cameras, in consumer electronics, and have a very low cost, in the range of few dollars. This is an advantage with respect to Application Specific Integrated Circuit (ASIC) designed ad-hoc for a specific application. Other advantages of this technology are the low power consumption, that it can work at room temperatures, and the possibility to have detectors with high spatial resolution, which have potential applications in different neutron techniques [17–19].

In this work we will show the implementation and the response of a thermal neutron detector based on a COTS CMOS image sensor covered with a coating which contains Gadolinium as a conversion layer. In Section 2, we will describe the proposed neutron detection technique, the sensor employed in this work, and the material used as conversion layer. In Section 3 we will describe the first experimental tests to prove the neutron detection capability of the proposed technique, and we will present additional experimental results in order to test the performance for conversion layers of different thicknesses. Finally in Section 4 we will discuss and analyze the relevance of the conclusions obtained in this work.

2. The neutron detection technique

In this section we introduce the proposed neutron detection technique, as well as the different components of the implemented experimental setup.

2.1. The CMOS sensors

The integrated circuit used in this work is an APTINA MT9V011 color CMOS image sensor, composed by 640 × 480 pixels with 5.6 μm × 5.6 μm pitch [20]. Fig. 1(a) shows a picture of the sensor employed in this work. The sensor is covered with a RGB Bayer pattern filter. In Refs. [15,16] we analyzed the response of this sensor to different kinds of ionizing particles. Fig. 1(b) and (c) shows a cross section of the sensor obtained using a Focused Ion Beam (FIB) and a Scanning Electron Microscope (SEM). After this analysis we observe that the silicon active area is covered with approximately 2.7 μm of insulating layer, and 3.9 μm of a polymer which form the Bayer filter. The region presented in Fig. 1(b) and (c) is the full range image obtained by FIB–SEM. The silicon active area of the sensor is thicker than that presented in Fig. 1, which is limited by the employed technique. More details on the structure of these sensors, as well as on their response to different ionizing particles can be found in Refs. [15,16]. All the measurements in this work were done acquiring 25 frames per second. The data acquisition, and processing were done using a standard PC without any special requirement, and the software was developed using Python and standard libraries.

2.2. The conversion layer

In order to be able to detect neutrons with this type of sensors, it is necessary to cover its surface with a conversion layer in which an intermediate nuclear reaction could take place. As was previously mentioned, conversion layers can contain different isotopes – for example ^{10}B, ^{6}Li,^{157}Gd, etc.– which, after the neutron capture, emit reaction products with stopping ranges of tens of micrometers in most solids [8]. Fig. 2 shows a scheme of the structure of the detector used in this work, which includes the layers that constitute the sensor, and the nuclear reaction. In order to be detected by the CMOS sensor, the emitted particles must have enough energy to get out of the conversion layer, cross the Bayer filter, the insulating layers that cover the chip, and reach the silicon active volume.

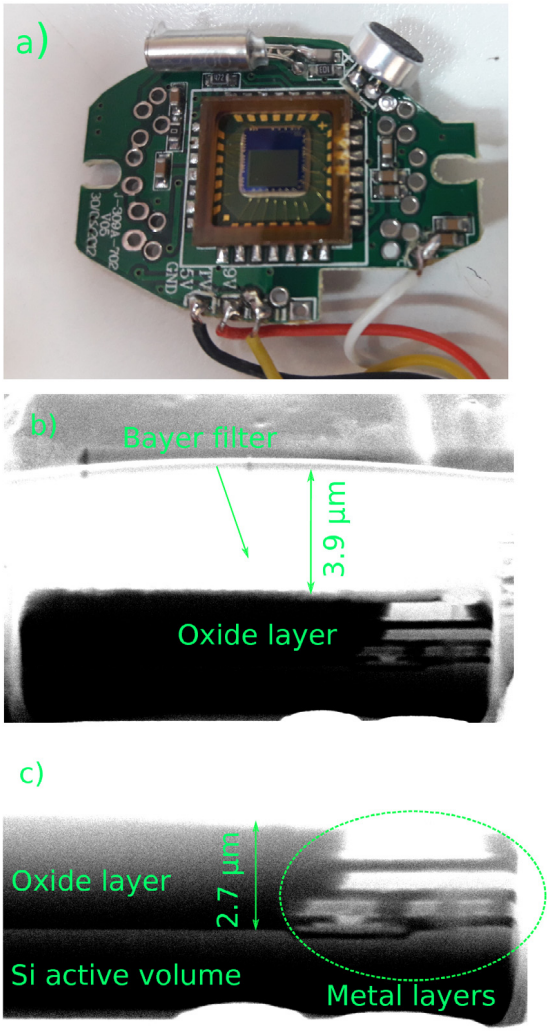

Fig. 1. (a) Picture of the CMOS sensor employed in this work. (b) Cross section of the sensor obtained using a Focused Ion Beam (FIB) and a Scanning Electron Microscope (SEM). The oxide layer, and the layer made on polymers which forms the color Bayer filter are indicated. (c) Zoom of the previous image where it can be seen the active area of the sensor and the layer of oxide and the metals of the chip [16].

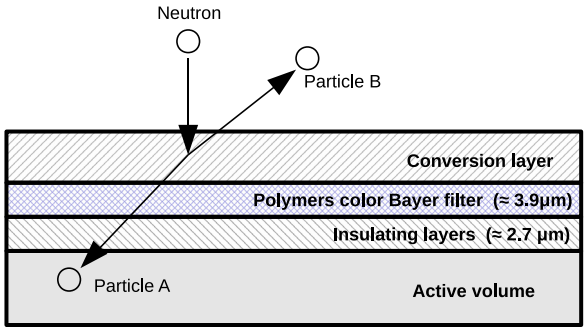

Fig. 2. Scheme of the layers present in the sensor used in this work, and the reaction produced in the conversion layer for a front irradiated configuration.

There is a conversion layer thickness that optimizes the neutron detection efficiency, which depends on the mean free path of the thermal neutrons into the employed material, and the range of the emitted

charged particles. On one hand, if the mentioned thickness is significantly smaller than the neutron mean free path, most of the neutrons will cross the conversion layer without interaction. On the other hand, if the conversion layer is notoriously thicker than the neutron mean free path, the neutron flux will be considerably attenuated. In this case, the range of the particles emitted after the nuclear reaction could limit the fraction of the conversion layer that will contribute to the signal. Therefore, a conversion layer significantly thicker than the neutron mean free path, and thicker than the range of the emitted charged particles, will also produce a low neutron detection efficiency. As was shown in Refs. [3,8], for a given conversion layer, the thickness that optimizes the neutron detection efficiency can be obtained numerically. For the specific case of a CCD device covered with ^{10}B, the thermal neutron mean free path, and the ranges of the reaction products produce neutron detection efficiencies lower than 3% [3]. To overcome this limitation, it has been proposed the use of multilayer detectors [21], a solution not possible with CMOS image sensors. In order to improve the detection efficiency for thermal neutrons, we employ a conversion layer made with Gd_2O_3. The thermal neutron capture cross section of natural Gd is 48,890 barns [22], which is greater than the 3820 barns for ^{10}B. The high cross section for natural Gd is mainly due to the isotope ^{157}Gd, which has 15.7% of natural isotopic abundance, and a thermal neutron absorption cross section of 255,000 barns. The reaction

$$n + {}^{157}_{64}Gd \rightarrow {}^{158}_{64}Gd^{*} \rightarrow {}^{158}_{64}Gd + \gamma + \text{conversion electron} \quad (1)$$

generates a cascade of gamma rays – approximately 3300 photons – , and an internal conversion electron (IC) [22]. If the $^{158}_{64}Gd^{*}$ decay to its ground state only by successive gamma decays, the total energy of the gamma rays emitted in this cascade would be 7937 keV [23]. However, the gamma cascade does not stop at the $^{158}_{64}Gd$ ground state, because an electron is emitted from the lowest two exited levels by the internal conversion process (IC). The IC electrons emitted have well defined energy lines – in the range of 29 to 246 keV– that depend on whether the IC is emitted from the K, L, or M shell. The three more probable lines are 71, 29, and 78 keV, which have a yield per absorbed neutron of 0.268, 0.098, and 0.061 respectively [24]. For the 71 keV IC electrons, the penetration depth in pure Gd has a distribution – which is analyzed in Ref. [24]– with a mean value of 5.03 μm, and a maximum penetration depth of 23.4 μm. From Ref. [24] it can be also seen that, in pure Si, the 71 keV electrons have a mean penetration depth of 21.0 μm, and a maximum penetration of 49.2 μm. The aim of this work, is to use the technique formerly presented for the detection of charged particles based on CMOS sensors [15,16] to measure the electrons emitted by Gd.

It is worth to mention that the events recorded by the sensor can be due to neutrons that interact with the conversion layer, as well as to background events. The background events could be produced, for instance, by gamma rays that interact with the sensor. In order to do a comparison under the same irradiation conditions, a fraction of the sensor active surface can be covered with the conversion layer, while the remaining part is left uncovered.

3. Experimental results

We have tested the proposed technique using different configurations. Firstly, we test a sensor partially covered with a Gadolinium containing conversion layer. Secondly, we evaluate the neutron detection efficiencies for conversion layers of different thicknesses.

3.1. Irradiation of a partially covered sensor

The first experimental test to prove the neutron detection capability of the proposed technique was to irradiate a sensor with its active area partially coated with a Gadolinium containing conversion layer. The employed material was made mixing Gd Oxide (Gd_2O_3) nanoparticles – particle dimensions smaller than 200 nm – , MicroPosit S1400 Series photo resist, and solvent. The Gd_2O_3 nanoparticles are available in the market since they are used for Magnetic Resonance Imaging applications [25,26]. A drop of the obtained mix was deposited on one half of the active area. The thickness of the obtained conversion layer is (5.1 ± 0.8) μm, which was measured using a mechanical profilometer. The sensor was irradiated using the neutron extraction tube N° 1 of the Nuclear Research Reactor RA6 located at Centro Atómico Bariloche, Argentina. This radial beam communicates the reactor core with a small neutron imaging instrument installed outside of the reactor pool [27]. The duct provides a beam formed by thermal neutrons, epithermal neutrons, and gamma rays of a wide range of energies. The neutron imaging facility has a closed enclosure where the samples can be irradiated. Fig. 3 shows the employed facility, and the implemented experimental setup inside the enclosure. In order to reduce the gamma field present in the employed radial extraction tube, a lead wall of 5 cm thickness was placed in front of the devices.

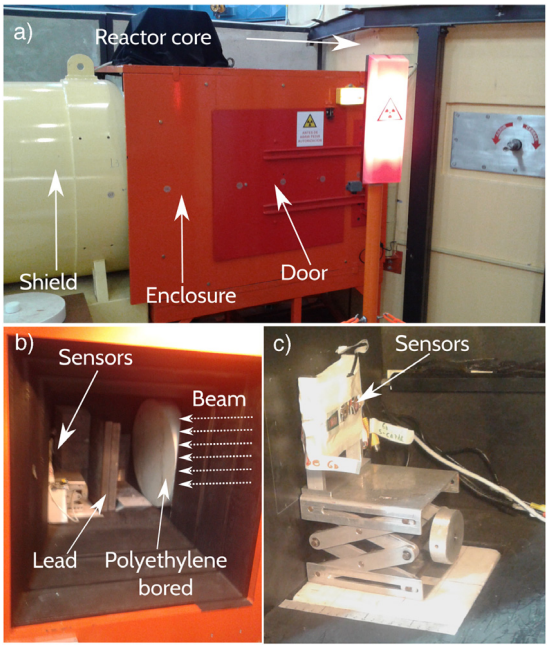

Fig. 3. (a) Neutron Imaging Facility of the RA6 Nuclear Research Reactor. (b) Experimental setup inside the closed enclosure. (c) Position of the sensors during the irradiations.

Fig. 4 shows a mesh plot of a typical event recorded on the sensor coated side with the conversion layer during a first irradiation. The inset of Fig. 4 depicts the image of this event using a gray-scale. After analyzing several events, it can be observed that the shape, the total collected charge, and the maximum intensity value are compatible with the values reported in previous works, in which we study the response of these sensors to beta particles, and gamma rays [15,16]. A counting process is possible after applying the method described in Refs. [15,16], which include a threshold value in order to discriminate the dark current contribution and the fixed pattern noise. Fig. 5 shows the total number of events detected on each pixel on a region of 100 × 100 pixels, obtained during 10 min at the mentioned irradiation conditions. The regions covered and not covered by the conversion layer can be clearly appreciated. Also, it can be seen that the mean number of recorded events in each pixel of the covered area – left side – is notoriously higher than that of the uncovered region. In the covered region the observed events are mainly due to neutrons that interact with the Gd of the conversion layer, as well as gamma rays that interact with the implemented device. On the uncovered region – right side – the observed events are mainly produced by gamma rays present in the beam. In Fig. 5, a transition zone of approximately 25 μm between both regions can be observed. The width of this transition zone depends on the spatial

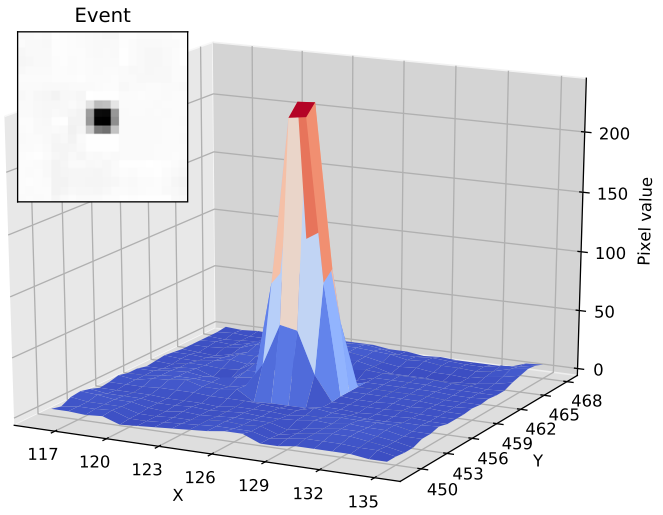

Fig. 4. Typical mesh plot of an event registered on the covered side of the sensor. The X and Y axis indicates the horizontal and vertical coordinates of each pixel. Inset: image of the event.

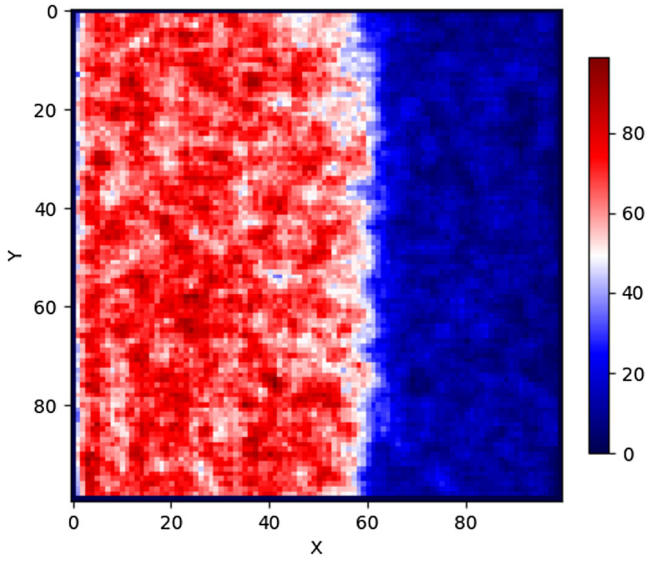

Fig. 5. Number of events detected on each pixel on a region of 100×100 pixels after an irradiation of 50 min. It can be clearly seen the limit between the covered –left – and the uncovered –right – regions.

resolution of the neutron detection technique introduced in this work, as well as on the sharpness of the Gd_2O_3 deposition border.

In order to analyze the capability of the implemented technique for neutron detection at different counting rates, we performed an irradiation cycle in which the reactor power was incremented in steps, stabilizing it at 15 kW, 50 kW, 150 kW, and 500 kW during time periods of approximately 10 min. Then, in order to attenuate the thermal and epithermal neutrons fluxes, a borated polyethylene block of 5 cm thickness was interposed into the beam, and irradiations at 500 kW and 150 kW were repeated. The borated polyethylene used to block the neutron beam can be observed in Fig. 3(b). Fig. 6 shows the counting rate obtained after processing the recorded events with the algorithm introduced in Refs. [15,16] as a function of the irradiation time. The presented results were obtained averaging 80 s of acquisition time. The counting rate was obtained with the mentioned algorithm on the zones covered and uncovered with Gd_2O_3. It can be seen that, for the applied power steps, the recorded counting rate increases monotonously. It is

Table 1
Atoms of Gd per cm^2 obtained by Rutherford Backscattering Spectrometry (RBS), and comparison of the conversion layers thicknesses obtained with a mechanic profilometer, and by RBS.

Number of layers	Atoms of Gd/cm^2	Thicknesses (μm)	
		Profilometer	RBS
2	$(320 \pm 5) \times 10^{16}$	5.7 ± 0.7	5.0 ± 0.5
3	$(545 \pm 5) \times 10^{16}$	7.9 ± 1.6	8.0 ± 0.8
5	$(730 \pm 10) \times 10^{16}$	11.1 ± 1.3	12.0 ± 1.3

worth to notice that the counting rate on the covered area at 500 kW is approximately 1.1×10^4 counts s^{-1} cm^{-2} and, when the neutron flux was attenuated by the borated polyethylene, it was reduced to approximately 0.05×10^4 counts s^{-1} cm^{-2}. It can also be observed that, when the borated polyethylene is present, the counting rate is almost the same on both sides of the sensor. The small difference observed for both counting rates could be due to neutrons not absorbed by the borated polyethylene. From the counting rates recorded with and without the borated polyethylene on the uncovered area, it was deduced that the borated polyethylene attenuates approximately 46% of the gamma contribution. Due to the thickness of the employed active volume – approximately 300 μm – this attenuation is mainly dominated by gamma photons with energies lower than approximately 500 keV, which have more probability to be detected than more energetic photons [28]. The results obtained in this section show the capability of the proposed technique to detect thermal neutrons. In the next section we present additional experimental results in order to analyze the performance of conversion layers with different thicknesses.

3.2. Conversion layer of different thicknesses

In order to standardize the deposition method, and to achieved a uniform dispersion of the applied layers by centrifugal force, a drop of the mixture described in Section 3.1 was deposited on the sensors, and then rotated at 3000 RPM for one minute using a spin coater. Then, the device was baked at 120 °C to evaporate the solvents. This procedure was repeated several times on the same sensor, thus obtaining a conversion layer of the desired thickness. Three different sensors, with 2, 3, and 5 layers have been made with the mentioned method. The thickness of the conversion layers was characterized by using a mechanical profilometer, and by Rutherford Backscattering Spectrometry (RBS) measurements carried out with protons produced by the Tandem Particle Accelerator located at Centro Atómico Bariloche [29,30]. Table 1 shows the obtained thicknesses for the three sensors tested in this section, as well as the number of atoms of Gd per cm^2 obtained by RBS. The standard deviations reported in Table 1 were obtained taking measurements at different points of each sensor. From the results of Table 1 it can be seen that the average thickness of each layer is approximately 2.5 μm.

The thermal neutron detection efficiencies for the conversion layers presented in Table 1 were experimentally obtained. For this purpose, a second irradiation cycle has been performed using the procedure and neutron beam detailed in Section 3.1. Fig. 7 shows the obtained counting rates for the three conversion layers with different reactor powers with and without the borated polyethylene shielding. It can be observed that – for the analyzed range – the counting rate increases with the conversion layers thickness. It is worth to note that, when the borated polyethylene is placed on the beam, the counting rate is almost the same for the three sensors. In this configuration the neutron flux is mainly attenuated by the borated polyethylene block, and therefore the recorded events are mostly produced by gamma rays. The small differences observed for the three counting rates could be due to neutrons not blocked by the borated polyethylene, which also produce more recorded events for the thicker conversion layers.

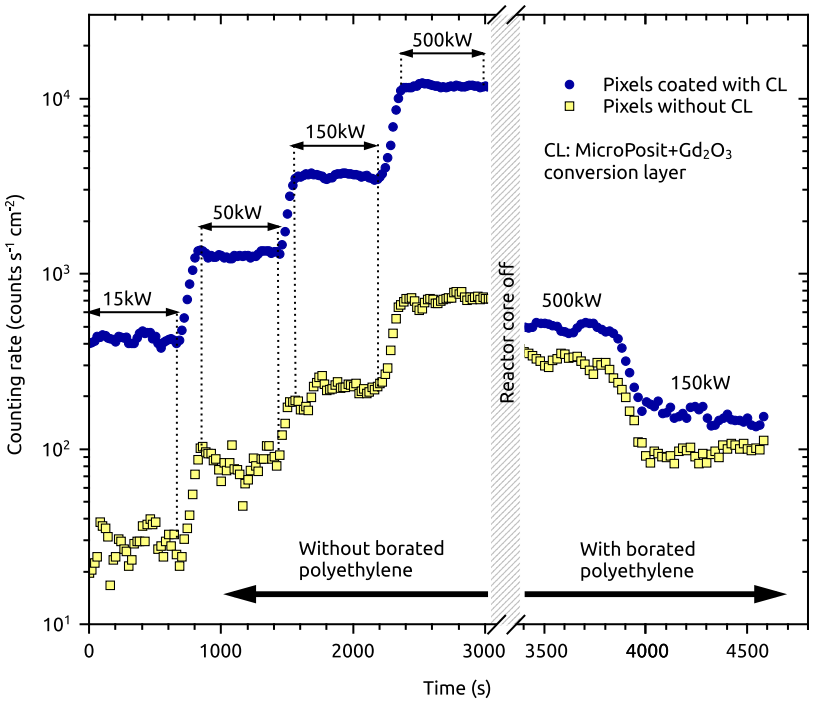

Fig. 6. Obtained counting rates in the uncoated region of a COTS CMOS sensor, and that in the region coated with a conversion layer made on a mix of MicroPosit S1400 and Gd_2O_3 nanoparticles as a function of the irradiation time. The power of the RA6 nuclear reactor during different time periods is indicated. In order to attenuate the incident neutron flux on the sensor, irradiations with an without a borated polyethylene were performed.

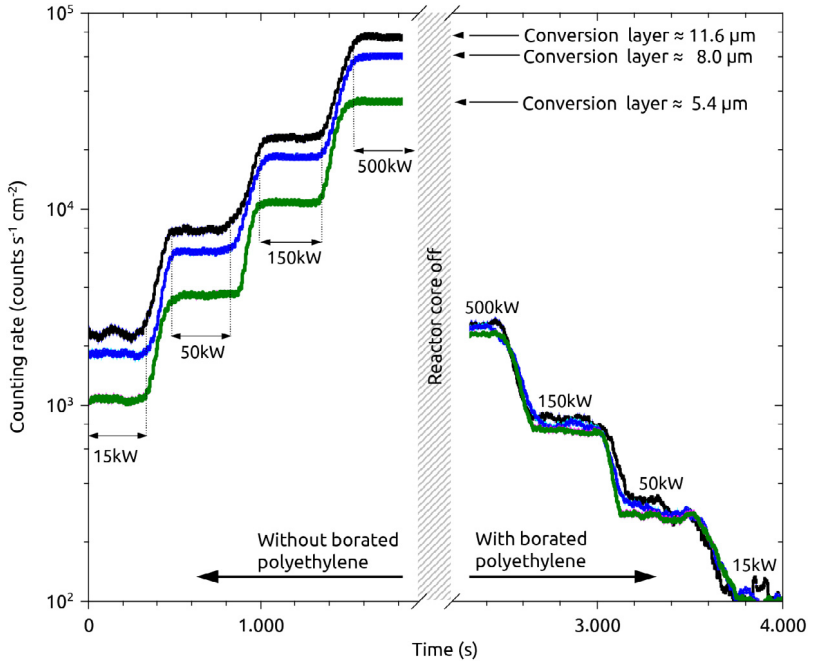

Fig. 7. Counting rates for the three conversion layers at different reactor powers, with and without the borated polyethylene shield.

The incident thermal neutron flux on the sensors is $(6.20 \pm 0.25) \times 10^5$ neutrons $cm^{-2}\,s^{-1}$. This flux was determined by the standard neutron activation analysis technique employing Mg/Au foils placed at the sensor position [31]. The rate of events due to neutrons has been obtained from the total recorded counting rate subtracting the gamma contribution. This gamma contribution was determined from the counting rate recorded with the borated polyethylene, taking into account the gamma attenuation obtained in Section 3.1. Fig. 8 shows the thermal neutron detection efficiencies obtained at different reactor powers. It is worth to notice that the obtained thermal neutron detection efficiencies are independent on the reactor power. This result shows that, for neutron fluxes lower than $(6.20 \pm 0.25) \times 10^5$ neutrons $cm^{-2}\,s^{-1}$, the neutron counting is not affected by saturation or dead time effects. The thermal neutron detection efficiencies obtained for the conversion layers

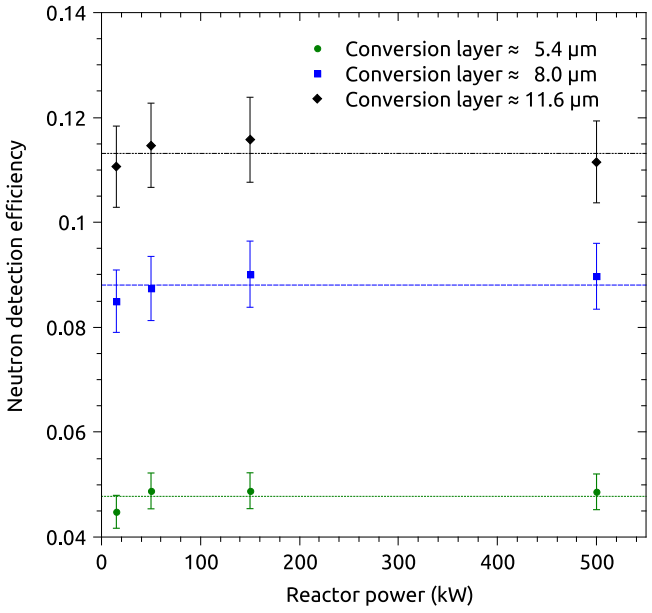

Fig. 8. Thermal neutron detection efficiencies obtained at different reactor powers for conversion layers of different thicknesses.

of 5.4 μm, 8.0 μm, and 11.6 μm are (4.8 ± 0.2)%, (8.8 ± 0.3)%, and (11.3 ± 0.4)% respectively. These values were obtained by averaging the results presented in Fig. 8.

4. Discussion and conclusions

A novel two-dimensional position sensitive technique for thermal neutron detection, using a CMOS image sensor and a conversion layer made on a Gd containing material, has been successfully implemented. As was shown in Section 3.1, the feasibility of the technique has been experimentally proved employing a sensor partially covered with Gd_2O_3. It is worth to notice that, when the implemented device was irradiated with thermal neutrons, the counting rate observed on the coated area was significantly higher than on the uncovered region. It was experimentally shown that the gamma contribution to the total counting rate can be experimentally obtained analyzing the uncovered zone of a partially coated sensor. Therefore, the gamma contribution can be subtracted from the total, thus obtaining the counting rate due to neutrons.

A method that allows an homogeneous deposition of Gd_2O_3 layers on the CMOS image sensor has been implemented. As can be seen in Section 3.2, for the front-irradiated configuration analyzed in this work, the experimentally observed neutron detection efficiency increases for thicker conversion layers. An efficiency of 11.3% has been achieved with a conversion layer of 11.6 μm. The probability of absorption of a thermal neutron in this layer can be estimated multiplying the number of Gd atoms per unit surface – 730×10^{16} atoms/cm^2 – with the neutron absorption cross section, yielding 35.6%. The 11.6% of overall efficiency implies that a third of the secondary electrons emitted by the conversion layer is finally detected as an event in the CMOS image sensor. This ratio between the neutron capture probability and experimental detection efficiency is constant for the three thicknesses. This result and the trend of the results presented in Section 3.2 imply that the neutron detection efficiency could be improved even more by using a conversion layer thicker than 11.6 μm. The formerly indicated efficiency is higher than the maximum value that could be achieved with a CCD device and conversion layers containing ^{10}B [3]. It was experimentally verified that the thermal neutron detection efficiency of the technique implemented in this work is independent on the reactor power, and therefore independent on the incident neutron flux. This result has been confirmed for the different conversion layer thicknesses tested in this work.

It is worth to point out that the neutron detection technique introduced in this work employs low cost CMOS image sensors. These COTS electronic devices are widely available in the market, and it does not have the commercial restrictions present nowadays for the neutron detectors based on ^3He. The reading-time of the CMOS imagers is significantly lower than that of a CCD device [32,33]. For this reason the CMOS devices are usually operated at room temperature, thus avoiding the need to employ a cryogenic system, being possible the acquisition of more than 20 frames per second. This characteristic allows dynamical studies that cannot be performed with a neutron detector based on a scientific CCD device [3].

It is also important to notice that, for natural Gd, the thickness that maximizes the thermal neutron detection efficiency is approximately 5 μm – see Fig. 6 of Ref. [22] – , which is compatible with the mean penetration depth of electron in natural Gd reported in Table 2 of Ref. [24]. Ref. [24] shows that the mean penetration depths of the electrons emitted after the neutron absorption in natural Gd, is also approximately 5 μm, and that the electron mean penetration depth increases for lower atomic numbers. Therefore, for the conversion layer employed in this work, made on a mixture of MicroPosit and Gd_2O_3, we expect a mean penetration depth greater than 5 μm. Besides, the neutron mean free path in the conversion layer employed in this work is greater than that of natural Gd [22]. For the two reasons formerly mentioned, the optimal thickness of the conversion layer employed in this work will be greater than 5 μm. This increase of the optimal thickness has been experimentally confirmed by the tendency of the results presented in Section 3.2, where we show that the neutron detection efficiency increases even for a conversion layer thicker than 11 μm.

Regarding the spatial resolution of the implemented technique, it is worth to remind that the distance between neighbor pixels is approximately 5.6 μm, which is comparable to the mean electron ranges previously mentioned. Therefore, the spatial resolution of the proposed technique is not only due by the electron ranges, but also by the interpixel distance. Besides, we must remember that into the sensor employed in this work, there is a SiO_2 layer, and a Bayer filter between the conversion layer and the active volume. Therefore, the electrons emitted in a direction almost parallel to the sensor surface are stopped into these intermediate layers. For this reason, the recorded events are produced by electrons emitted almost normally to the sensor surface, and the spatial resolution is improved.

It is worth to remember that the thickness of the transition zone between the coated and uncoated areas shown in Fig. 5 – approximately 25 μm – is not only due to the spatial resolution of the technique introduced in this work, but also by the sharpness of the border of the deposited conversion layer. Therefore, for the technique introduced in this work, we expect a spatial resolution better than 25 μm, which is comparable with that obtained employing the detection techniques with the highest spatial resolutions achievable nowadays [3,34–37]. Due to the high spatial resolution reached with this technique, and the fact of use low cost COTS sensors, it can be a convenient option for neutron beam characterization, neutron dosimetry, and will have several applications on different neutron based experimental techniques, for example Compact SANS [5], Neutron Imaging [35], and Neutron Reflectometry [6].

Acknowledgments

This work was supported by ANPCyT under projects PICT 2014-1966 and PICT-2015-1644, UNCuyo C018, and by CONICET under projects PIP 20110552 and PIP 2013-0077. The authors would like to thank to the RA6 staff, Julio Marin and Juan Longhino for their help during neutron irradiations; the CMB-INTI for the use of the FIB; and Julian Azcárate, Leonardo de Jesus Zalazar and Manuel Gonzalez for their help in the cleanroom.

References

[1] R.T. Kouzes, J.H. Ely, L.E. Erikson, W.J. Kernan, A.T. Lintereur, E.R. Siciliano, D.L. Stephens, D.C. Stromswold, R.M. Van Ginhoven, M.L. Woodring, Neutron detection alternatives to ^{3}He for national security applications, Nucl. Instrum. Methods Phys. Res. A 623 (3) (2010) 1035–1045.

[2] D.A. Shea, D. Morgan, The helium-3 shortage: Supply, demand, and options for Congress, in: Congressional Research Service, Library of Congress, 2010.

[3] J.J. Blostein, J. Estrada, A. Tartaglione, M.S. Haro, G.F. Moroni, G. Cancelo, Development of a novel neutron detection technique by using a boron layer coating a charge coupled device, J. Instrum. 10 (01) (2015) P01006.

[4] A. Cho, Helium-3 shortage could put freeze on low-temperature research, Science 326 (5954) (2009) 778–779.

[5] L. Feigin, D.I. Svergun, et al., Structure Analysis by Small-Angle X-Ray and Neutron Scattering, Springer, 1987.

[6] J. Daillant, A. Gibaud, X-Ray and Neutron Reflectivity: Principles and Applications, Vol. 770, Springer, 2008.

[7] M. Trocmé, S. Higueret, D. Husson, A. Nourreddine, T. Lê, A new compact device for efficient neutron counting using a CMOS active pixel sensor, Radiat. Meas. 43 (2) (2008) 1100–1103.

[8] D.S. McGregor, M. Hammig, Y.-H. Yang, H. Gersch, R. Klann, Design considerations for thin film coated semiconductor thermal neutron detectors I: basics regarding alpha particle emitting neutron reactive films, Nucl. Instrum. Methods Phys. Res. A 500 (1) (2003) 272–308.

[9] R. Nikolić, C.L. Cheung, C. Reinhardt, T. Wang, Future of Semiconductor Based Thermal Neutron Detectors, Barry Chin Li Cheung Publications, 2006, p. 14.

[10] E.H. Lehmann, P. Vontobel, G. Frei, C. Brönnimann, Neutron imaging detector options and practical results, Nucl. Instrum. Methods Phys. Res. A 531 (1) (2004) 228–237.

[11] C. Guardiola, C. Fleta, G. Pellegrini, F. García, D. Quirion, J. Rodríguez, M. Lozano, Ultra-thin 3D silicon sensors for neutron detection, J. Instrum. 7 (03) (2012) P03006.

[12] D.E. Pooley, J.W.L. Lee, M. Brouard, J.J. John, W. Kockelmann, N.J. Rhodes, E.M. Schooneveld, I. Sedgwick, R. Turchetta, C. Vallance, Development of the 'GP2' detector: Modification of the PImMS CMOS sensor for energy-resolved neutron radiography, IEEE Trans. Nucl. Sci. 64 (12) (2017) 2970–2981. http://dx.doi.org/10.1109/TNS.2017.2772040.

[13] J. Uher, C. Frojdh, J. Jakubek, C. Kenney, Z. Kohout, V. Linhart, S. Parker, S. Petersson, S. Pospísil, G. Thungstrom, Characterization of 3D thermal neutron semiconductor detectors, Nucl. Instrum. Methods Phys. Res. A 576 (1) (2007) 32–37.

[14] R. Nikolic, C.L. Cheung, C. Reinhardt, T. Wang, Roadmap for high efficiency solid-state neutron detectors, in: Optics East 2005, International Society for Optics and Photonics, 2005 601305–601305.

[15] M. Pérez, J. Lipovetzky, M.S. Haro, I. Sidelnik, J.J. Blostein, F.A. Bessia, M.G. Berisso, Particle detection and classification using commercial off the shelf CMOS image sensors, Nucl. Instrum. Methods Phys. Res. A 827 (2016) 171–180.

[16] M. Pérez, M.S. Haro, I. Sidelnik, L. Tozzi, D.R. Brito, C. Mora, J.J. Blostein, M.G. Berisso, J. Lipovetzky, Commercial CMOS pixel array for beta and gamma radiation particle counting, in: Micro-Nanoelectronics, Technology and Applications, EAMTA, 2015 Argentine School of, IEEE, 2015, pp. 11–16.

[17] G. Cuello, J. Dawidowski, J. Granada, J. Santisteban, J. Blostein, L.R. Palomino, Proposal for instruments at small and medium size neutron facilities, J. Phys.: Conf. Ser. 325 (1) (2011) 012013.

[18] A. Tartaglione, J. Blostein, F. Cantargi, J. Marín, A. Baruj, G. Meyer, J. Santisteban, F. Sánchez, Present and future activities on neutron imaging in argentina, Phys. Procedia 69 (2015) 124–129.

[19] F. Fernandez-Alonso, D.L. Price, Neutron Scattering, Vol. 44, Academic Press, 2013.

[20] On semiconductor, http://www.onsemi.com. Accessed 23 February 2018.

[21] T. Kawai, T. Ebisawa, S. Tasaki, H.M. Shimizu, An improvement of the detection efficiency of a solid state UCN detector with a ^{6}Li/Ti multilayer neutron converter working at liquid helium temperature, Nucl. Instrum. Methods Phys. Res. A 378 (3) (1996) 561–563.

[22] D. Abdushukurov, M. Abduvokhidov, D. Bondarenko, K.K. Muminov, T. Toshov, D.Y. Chistyakov, Modeling the registration efficiency of thermal neutrons by gadolinium foils, J. Instrum. 2 (04) (2007) P04001.

[23] R.B. Firestone, V.S. Shirley, C.M. Baglin, et al., Table of Isotopes CD-ROM, Version 1, eight ed., 1996.

[24] P. Kandlakunta, L. Cao, P. Mulligan, Measurement of internal conversion electrons from Gd neutron capture, Nucl. Instrum. Methods Phys. Res. A 705 (2013) 36–41.

[25] D. Miller, P. Rudge, G. Johnson, B. Kendall, D. Macmanus, I. Moseley, D. Barnes, W. McDonald, Serial gadolinium enhanced magnetic resonance imaging in multiple sclerosis, Brain 111 (4) (1988) 927–939.

[26] L. Kappos, D. Moeri, E.W. Radue, A. Schoetzau, K. Schweikert, F. Barkhof, D. Miller, C.R. Guttmann, H.L. Weiner, C. Gasperini, et al., Predictive value of gadolinium-enhanced magnetic resonance imaging for relapse rate and changes in disability or impairment in multiple sclerosis: a meta-analysis, The Lancet 353 (9157) (1999) 964–969.

[27] J. Marín, F. Sánchez, H. Blaumann, Rediseño, construcción y caracterización de la nueva instalación de neutrografía del RA-6. Revista de la CNEA 49/50.

[28] G.F. Knoll, Radiation Detection and Measurement, John Wiley & Sons, 2010.

[29] S. Limandri, C. Olivares, L. Rodriguez, G. Bernardi, S. Suárez, Pixe facility at centro atómico bariloche, Nucl. Instrum. Methods Phys. Res. B 318 (2014) 47–50.

[30] M. Mayer, SIMNRA: Computer Simulation of RBS, ERDA and NRA (With License Number in Name of Sergio Suárez), Max-Planck-Institut für Plasmaphysik. http://home.mpcdf.mpg.de/~mam/index.html.

[31] N.F. Measurements, IAEA Technical Reports Series N°. 107, IAEA, VIENNA, 1970.

[32] J.R. Janesick, Scientific Charge-Coupled Devices, Vol. 83, SPIE press, 2001.

[33] E. Tiouchichine, M.S. Haro, X. Bertou, H. Amaldi, M.G. Berisso, J. Blostein, J. Tiffenberg, M. Pérez, S. Suárez, G.F. Moroni, Setup and calibration of a particle detector based on charge coupled devices, in: Micro-Nanoelectronics, Technology and Applications, CAMTA, 2017 Argentine Conference of, IEEE, 2017, pp. 5–9.

[34] B. Guerard, R. Hall-Wilton, F. Murtas, Prospects in MPGDs development for neutron detection, 2014. ArXiv preprint arXiv:1410.0107.

[35] I.S. Anderson, R.L. McGreevy, H.Z. Bilheux, Neutron imaging and applications, Springer Sci. Bus. Media 200 (2209) (2009) 987–0.

[36] A.S. Tremsin, W.B. Feller, R.G. Downing, Efficiency optimization of microchannel plate (MCP) neutron imaging detectors. I. Square channels with ^{10}B doping, Nucl. Instrum. Methods Phys. Res. A 539 (1) (2005) 278–311.

[37] A. Tremsin, J. Vallerga, J. McPhate, O. Siegmund, W. Feller, L. Crow, R. Cooper, On the possibility to image thermal and cold neutron with sub-15μm spatial resolution, Nucl. Instrum. Methods Phys. Res. A 592 (3) (2008) 374–384.